Proceedings of the Combustion Institute, Volume 28, 2000/pp. 991–997

EXPERIMENTAL STUDY OF NONANE/HEXANOL MIXTURE DROPLET COMBUSTION WITHOUT NATURAL OR FORCED CONVECTION

C. THOMAS AVEDISIAN AND BRIAN J. CALLAHAN
Sibley School of Mechanical and Aerospace Engineering
Cornell University
Ithaca, New York 14853-7501, USA

In this paper we present new data on the combustion of stationary nonane/hexanol mixture droplets burning in microgravity to promote spherical symmetry. Compositions of 10%, 25%, 40%, 60%, and 80% (volume percent hexanol) were examined in a drop tower to create an environment whereby droplets could burn without a strong influence of buoyancy. The evolution of droplet, soot shell, and flame diameter were measured, and photographs are presented to show sooting trends as composition was varied. Droplets with initial diameters between 0.46 mm and 0.57 mm were studied.

The results show that dilution of nonane by hexanol reduces soot formation and decreases the droplet burning rate, the latter of which was found to be time dependent. Mechanisms for this effect which are considered include soot formation, the potential for absorption of combustion products in the droplets as they burn, and droplet heating. Because of the similarity of the boiling points of the mixture components, preferential vaporization did not occur. The droplets burned to completion, and extinction was not observed because of minimal radiative losses for the small droplet sizes examined and low propensity for water to condense on the droplet surface and dissolve in it for nonane and hexanol.

A soot shell was not visible for hexanol loadings above 10%. The flame and soot shell standoff ratios increased continuously during burning. The flame diameter showed no sign of a quasi-steady behavior at any time during the combustion process. As hexanol concentration was increased, the flame moved toward the droplet.

Introduction

One of the most important problems for a clean environment is the ability to predict and control soot formation and particulate emissions in liquid fuel combustion processes. This capability is currently prohibitive for spray combustion because of the complex swirling/turbulent flow patterns and the droplet interactions involved. A benchmark liquid fuel burning configuration is more attractive for constructing and testing a predictive framework for soot formation. Spherically symmetric droplet combustion is such a benchmark because of its one-dimensional flow field. Experimental results from this droplet burning configuration will be important to evaluate numerical simulations of this problem.

We report new measurements of the evolution of droplet, soot shell, and outer luminous zone (i.e., flame) diameter of nonane/hexanol (C_9H_{20}/$C_6H_{15}OH$) mixture droplets burning in low gravity to promote gas-phase spherical symmetry in the droplet combustion process. The initial droplet diameter (D_o) was kept within a narrow range of 0.46 mm $< D_o <$ 0.57 mm. Nonane is highly sooting while hexanol produces minimal soot, so that an influence of composition on soot formation could be readily observed by varying the composition. The compositions studied were hexanol volume percents of 10%, 25%, 40%, 60%, and 80%.

Spherically symmetric combustion of sooting pure fuel droplets has received significant attention [1–8], and so have studies of mixture droplets in which the components are composed of both miscible and immiscible fuels [9–17]. Measurements of the evolution of droplet and flame diameter are the most common. A soot shell is a prominent feature of spherical droplet flames [18] but measurements of its diameter are scarce for single-component droplets [5,6], and no data are known for mixture droplets.

The nonane/hexanol combination is interesting as a model mixture system because burning for this mixture should be a simplified process. Nonane and hexanol are not strongly soluble in water [19,20], and their boiling points (431 K for hexanol and 424 K for nonane [21]) are high enough so that condensation of water should not be important for the influence it could have on the burning rate and extinction [22,23]. The properties of nonane, hexanol, and their mixtures are readily predicted by standard methods [24], which is useful for modeling purposes. Because of the small values of D_o examined here, radiative or conductive heat losses [5,9,25–27] should not be important.

The diagnostic we used consisted of video and 16 mm high-speed cameras. While more quantitative methods are starting to be used to probe sooting

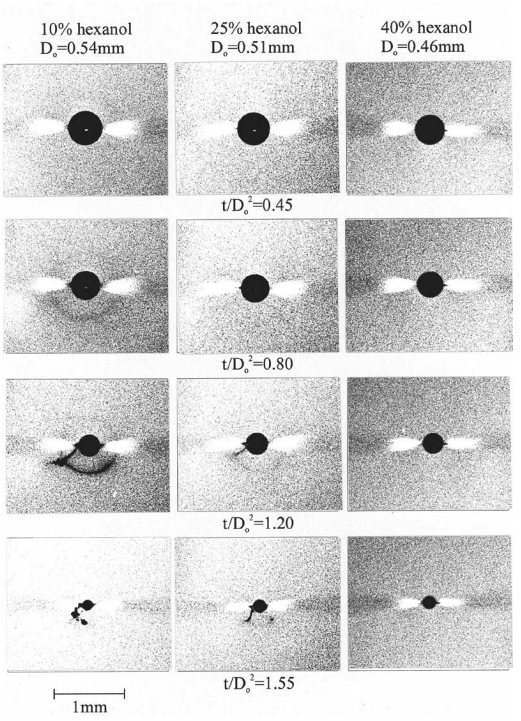

FIG. 1. Photographs of nonane/hexanol mixture droplets supported on a 12 μm fiber and burning in low gravity. White regions are the glow from the flame-fiber interactions. Trapped soot is visible for the 10% concentration at $t/D_o^2 = 1.2$ s/mm^2.

spherical droplet flames [17,28,29], the present study emphasizes the evolution of droplet and soot shell diameters and visualizations of the structure of the mixture droplet flames. Backlighted photography is an acceptable quantitative tool for this purpose.

Description of the Experiment

The experiments were performed in low gravity to minimize buoyancy. A drop tower with a drag shield created gravity levels that were less than 10^{-4} of Earth's normal gravity (9.8 m/s^2). When coupled with the small initial droplet diameters studied, the dynamic range of parameters combined [27,30] to promote spherical gas-phase symmetry and a burning process that could be completed in the time available for the experiment.

Because we experienced difficulties using a prior free droplet design [2,6,13,30] to keep unsupported nonane/hexanol mixture droplets from moving while they burned, we designed a new fiber support arrangement to anchor the test droplets. A modification of a stretched fiber support design [31,32] was used. Two 12 μm SiC fibers ($D_{fiber} = 12$ μm) were stretched across four posts in a crossing pattern at an angle of about 17°. Droplets with approximately $38 < D_o/D_{fiber} < 48$ were examined to minimize the fiber's influence on burning, which could be substantial for sooting fuel droplets [33]. The procedure for placing small droplets on these small fibers was to aim a piezoelectric droplet generator [2] at the intersection of the two fibers. As the droplet hit the cross, it stuck to it. The droplet diameter of interest was built up by impingement and successive coalescences of droplets, similar to the process carried out previously [6] for placing droplets at the tip of a single fiber. With the test droplet hanging from the cross of the fibers, the package which houses the combustion chamber with droplet and associated hardware was then released into free fall, after which the droplet was ignited and its burning history recorded.

The total experimental run time was 1.2 s for a 7.6 m free-fall. For the droplet diameters studied in this work, typical burning times were under 0.5 s. Two sparks of 0.5 ms duration positioned on opposite sides of the droplet, with a gap of 2.5 mm and located 3.5 mm away from the droplet center, were activated 0.5 s after the period of free fall. This delay period allowed visible droplet oscillations to subside, and it helped mitigate internal liquid flows which can be created by droplet deployment in microgravity experimentation [34].

Comparing pure nonane droplet combustion using the fiber support arrangement described above to free nonane droplet results showed excellent agreement [35] concerning the evolution of droplet diameter. This agreement gave confidence that results from the fiber-supported experiments discussed here would be close to the free-droplet results of nonane/hexanol mixtures of similar size and composition.

A high-speed movie camera was operated at 200 frames/s using a LOCAM II 16 mm camera fitted with an Olympus 90 mm Zuiko lens and extension bellows. A second camera, a COHU 8295 color video camera (60 frames/s) was mounted perpendicularly to the 16 mm movie camera to record the droplet position along the perpendicular view axis of the movie camera. The film images were digitized on a Microtek slide scanner at 3900 dpi, and then imported into *Image Pro-Plus* (V. 4.0) (Media Cybernetics). The software finds the edge of the droplet by categorizing the pixels according to a threshold brightness.

Discussion

Photographs of Nonane/Hexanol Mixture Droplets

Figure 1 shows a series of black and white prints of fiber-supported nonane/hexanol mixture droplets

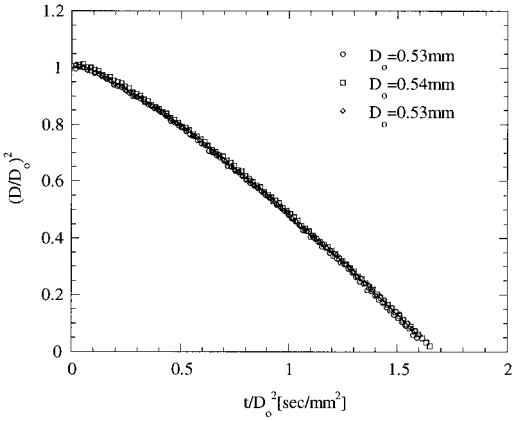

FIG. 2. Evolution of scaled droplet diameter, $(D/D_o)^2$, with scaled time, t/D_o^2, for 10% hexanol in nonane droplets. Initial droplet diameters are shown in the inset.

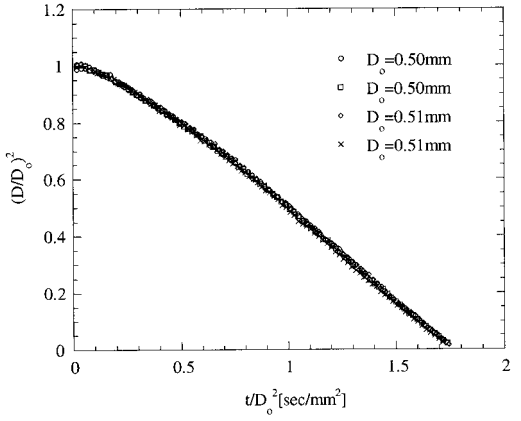

FIG. 3. Evolution of scaled droplet diameter, $(D/D_o)^2$, with scaled time, t/D_o^2, for 25% hexanol in nonane droplets. Initial droplet diameters are shown in the inset.

burning in microgravity containing initially 10%, 25%, and 40% hexanol. Higher concentrations of hexanol showed no visual differences from the 40% concentration. Because the backlight intensity and photo processing were identical, the image variations are a true indication of hexanol's influence on soot formation. A soot shell is visible only for 10% hexanol droplets, and then only faintly so, which is in stark contrast to pure nonane, which had intense soot shells [35]. This shows the strong influence that hexanol has on the reduction of sooting through a dilution or chemical effect [36,37] by the comparatively non-sooting tendency of hexanol.

Color video images, not shown here, revealed that 10% hexanol droplets had a bright yellow inner flame and much dimmer outer blue flame. At 60% hexanol, the flame image was almost entirely blue

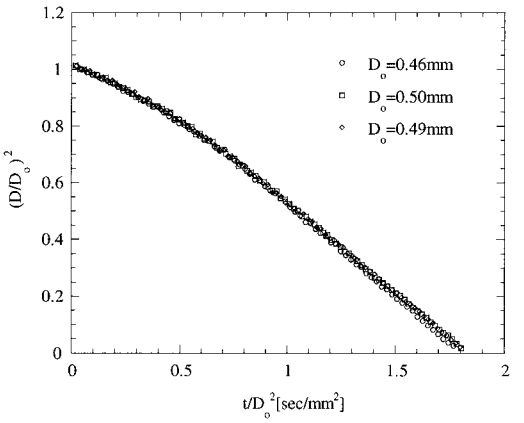

FIG. 4. Evolution of scaled droplet diameter, $(D/D_o)^2$, with scaled time, t/D_o^2, for 40% hexanol in nonane droplets. Initial droplet diameters are shown in the inset.

with just a hint of yellow, and at 80% there was no evidence of any yellow in the color video image.

Evolution of Droplet Diameter

The evolution of droplet diameter is presented in scaled coordinates from the quasi-steady state theory of droplet combustion [36], namely that a plot of $(D/D_o)^2$ against t/D_o^2 should be a straight line with slope $K \equiv -d(D^2)/dt$, which does not depend on time. This scaling is also valid for miscible mixtures with proper descriptions of the properties expressed in terms of composition [38]. The flame front standoff ratio (D_f/D) should be constant by the quasi-steady theory. (Flame diameter data are discussed in the next section.)

Figures 2–4 show the variation of $(D/D_o)^2$ with t/D_o^2 for 10%, 25%, and 40% nonane/hexanol mixtures. The trends are typical of higher concentrations, which are not shown because of space limitations. For each composition, the experiment was repeated three or four times. The repeatability was excellent. Extinction is not evidenced because neither nonane nor hexanol absorbs water significantly [19,20], and the initial droplet diameter is too small for radiation to be an important heat loss mechanism [9,25–27].

As shown in Figs. 2–4, the evolution of D^2 is not linear. The burning rate increases as time progresses, which is more clearly seen in Fig. 5, which displays the evolution of the instantaneous burning rate. The burning rates were extracted from data like those shown in Figs. 2–4 by differentiating each smoothed variation of $(D/D_o)^2$ with t/D_o^2 and then fitting them with a logarithmic function. Integration of each curve shown in Fig. 5 reproduced very well the original experimental data sets from which they were obtained. It was found that the burning rates for the 40% and 60% mixtures were almost identical.

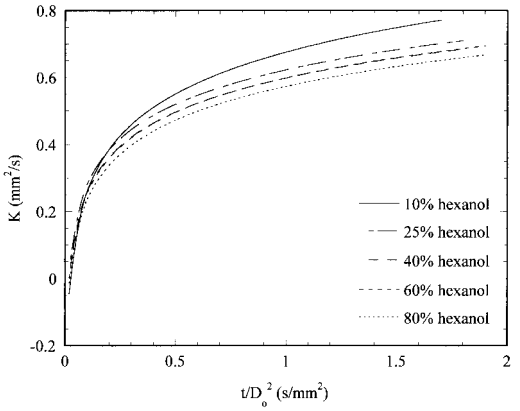

FIG. 5. Variation of instantaneous burning rate with scaled time for nonane/hexanol mixture droplets. Initial compositions are listed in the inset. The variations were obtained from curve-fits of data like those shown in Fig. 2–4. Note that the burning rate decreases as hexanol concentration increases.

For a given initial concentration, there are several mechanisms for a time-dependent burning rate. These include radiative losses (which are not expected to be important, as noted previously), soot formation, absorption of pyrolysis products in the droplet during burning, and droplet heating. Concerning the role of soot formation, as the droplet evaporates, the fuel molecule residence time decreases [30] so that less soot should form. With reduced soot formation should come a higher chemical energy release at the flame, more heat transfer to the droplet, and a higher burning rate. It is noted that combustion of several other sooting fuels showed a nonlinear D^2 progression for burning at atmospheric pressure [6] and 0.5 atm [39]. In the present study, a soot shell was not observed above about the 10% hexanol concentration, yet burning was still nonlinear even for very heavy hexanol loadings, as shown in Fig. 5. This result shows that for the nonane/hexanol mixtures examined, soot formation is probably not the cause of nonlinear burning.

It has been speculated [40] that low-volatility pyrolysis products can dissolve into a burning droplet to transform an initially single-component droplet into a multicomponent droplet. Such absorption can also lead to preferential vaporization. Because the burning rate is determined somewhat by the vaporizing component, a continuously changing burning rate and nonlinear D^2 progression could be realized because of the presence of the dissolved combustion products. If the dissolved impurities have low volatility, secondary atomization or microexplosion could also occur; however, it was not observed for any of the mixture droplets examined. Further experiments would have to be performed to sample droplets at various times during combustion to analyze their composition in order to prove the viability of this mechanism for nonlinear burning.

The manifestation of droplet heating is a burning rate which increases with time. An energy balance at the droplet surface can be expressed as (neglecting radiation) [38] $\Lambda = 1 + \delta_{d,f}$ where

$$\delta_r = \frac{C_{pL} D}{6 h_{fg}} \left.\frac{dT}{dr}\right|_{r=D/2}$$

or

$$\delta_d = \frac{4 k_L D}{\rho_L h_{fg} K} \left.\frac{dT}{dr}\right|_{r=D/2}$$

depending on if diffusion occurs inside the droplet (δ_d) or the droplet interior is well mixed (δ_r). Here, C_{pL}, h_{fg}, ρ_L, and k_L are the liquid specific heat, heat of vaporization, liquid density, and liquid thermal conductivity, respectively. Unless δ_d or $\delta_r \ll 1$, droplet heating will occur and the burning rate will depend on time. Scaling the derivative as

$$\left.\frac{dT}{dr}\right|_{r=D/2} \approx \frac{T_b - T_i}{D/2}$$

where T_b is the fuel boiling point and T_i is the initial droplet temperature (about 300 K), then

$$\delta_r \approx \frac{C_{pL} (T_b - T_i)}{3 h_{fg}}$$

and

$$\delta_d \approx \frac{8 k_L (T_b - T_i)}{\rho_L h_{fg} K}$$

For hexanol and nonane, δ_d and δ_r range between 0.25 and 1.0 using reasonable property estimates [24]. Therefore, droplet heating is viable.

In addition to soot formation, which we have already speculated does not influence burning for the mixtures studied, increasing the hexanol concentration increases the mixture liquid density (ρ_L) because hexanol has a higher liquid density than nonane (e.g., room temperature values of 815 kg/m^3 for hexanol compared to 718 kg/m^3 for nonane [21]). The quasi-steady theory of burning [36] shows that $K \propto 1/\rho_L$. Since hexanol has a higher liquid density than nonane, the droplet should burn more slowly and the burning time should increase as hexanol is added, which is also consistent with Fig. 5. Hexanol concentration also alters the position of the flame relative to the droplet, which is discussed in the next section.

Neither preferential vaporization nor a plateau is evident in Figs. 2–4 because nonane and hexanol have the same boiling points at the combustion pressure (1 atm). The fact that the vapor pressures of both nonane and hexanol are the same at the pressure under which the experiments were performed

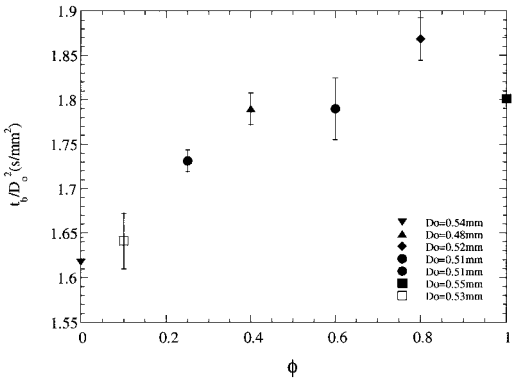

FIG. 6. Influence of t_b/D_o^2 with initial composition (volume fraction, ϕ) where t_b is the burning time corresponding to $D = 0$, as determined from data like those shown in Figs. 2–4. Each data point represents an average value of at least three repetitions. The error bars show the standard deviation. The average initial droplet diameters are shown in the inset. Hexanol has the greatest effect on burning time for dilute concentrations.

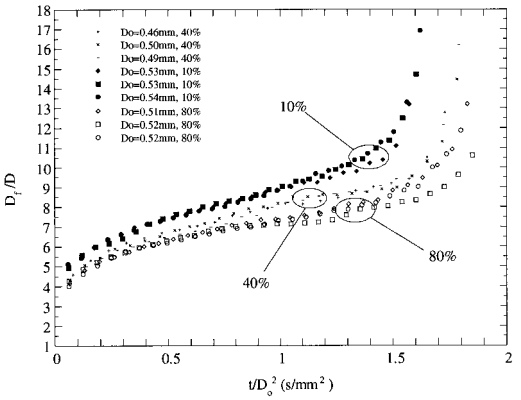

FIG. 7. Variation of flame (i.e., outer luminous zone) standoff ratio, D_f/D, with scaled time, t/D_o^2, for three compositions. Instantaneous droplet diameters, $D(t)$, were obtained from separate D^2 measurements. Quasi-steady burning is never achieved during the droplet lifetime. As hexanol concentration is increased, the flame moves closer to the droplet.

(1 atm) then also makes preferential vaporization unlikely, which is consistent with the D^2 progressions for all the compositions examined. The droplet composition then does not change during burning, which would make for a simplified analysis of this sooting mixture system.

Figure 6 shows the variation of t_b/D_o^2 with volume fraction, where t_b is the burning time at which D = 0 as determined from data similar to those shown in Figs. 2–4. Mean values are presented, and the bars show the standard deviations due to the small variations of D_o for each of the compositions examined, as well as the intrinsic uncertainties in the measurements. t_b/D_o^2 varies with composition because of the liquid density influence on burning rate noted previously and hexanol's effect on the proximity of the flame to the droplet as discussed in the next section. As illustrated in Fig. 6, adding hexanol to nonane increases t_b/D_o^2, which follows the reduction of K shown in Fig. 5. The influence is strongest at low hexanol loadings and diminishes at high hexanol concentrations.

Flame Standoff Ratio

Figure 7 compares the variation of D_f/D with t/D_o^2 for 10%, 40%, and 80% nonane/hexanol mixture fractions. Other compositions were placed in between the data shown in Fig. 7 but were not presented so as not to clutter the figure. The measurements are of the outer luminous zone of the video images and show little scatter. Experiments were repeated three times for each composition, and the repeatability was very good. Accurate measurement of the flame diameter is more difficult than of the droplet diameter because the luminous zone diameter is less well defined than the droplet diameter. The scatter inherent in the measurements shown in Fig. 7 is due to this less well defined boundary. The initial droplet diameter was in the range of 0.49 mm to 0.54 mm, which is essentially constant and should not influence the burning process. The value of D to determine the ratio D_f/D was determined by taking the instantaneous droplet diameter from data like those shown in Fig. 2–4 corresponding to the time of the flame diameter measurement.

As shown in Fig. 7, the flame standoff ratios are not constant. Together with the time-varying burning rate shown in Fig. 5, the nonane/hexanol droplet burning process is clearly not quasi-steady. D_f/D starts low, levels off somewhat during the middle period of burning, and finally tails up at the end. As hexanol concentration increases, the flame is pulled closer to the droplet surface, as shown in Fig. 7. With the closer flame position, the fuel molecule residence time is reduced [30], which also reduces soot formation.

Soot Shell Standoff Ratio

Figure 8 shows the soot shell standoff ratio, D_s/D, for 10% hexanol droplets. Unfortunately, higher hexanol concentrations showed no visible soot. The data in Fig. 8 span only the central portion of burning because of the delay time for soot formation early on. Soot formation is not important in the later period of burning because of the smaller droplet diameter and reduced soot formation that results [12,13]. Soot collection on the fiber also sometimes

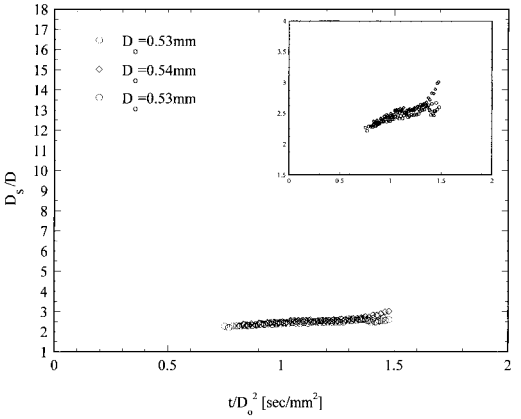

FIG. 8. Measurements of the soot standoff ratio, D_s/D, with scaled time, t/D_o^2, for 10% hexanol-in-nonane droplets. Initial droplet diameters are shown in the inset. At higher hexanol concentrations and early times, the soot shell was too faint to allow reliable measurements of D_s. The soot shell resides between the droplet ($D_s/D = 1$) and the flame (i.e., compare with Fig. 7).

made a shell image an incomplete circle in the data processing method. D_s was difficult to measure under these circumstances.

As shown in Fig. 8, there is a slight increase of the soot standoff ratio with time. This trend tracks with the flame standoff ratio shown in Fig. 7 and is consistent with previous measurements of D_s/D for heptane and chloro-octane droplets [6]. In all cases, the soot shell formed on the fuel-rich side of the flame, as shown in Figs. 7 and 8.

Summary

1. For a given initial concentration, the time-dependent burning rate is most likely linked to a combination of pyrolysis product absorption in the droplet and droplet heating, but probably not to soot formation because droplets with high hexanol concentrations also showed a time-dependent burning rate.
2. Hexanol addition increases the liquid density and lowers the flame temperature, which in turn lowers the burning rate. The flame diameter is also reduced, the fuel molecule residence time decreases, and less soot forms.
3. Quasi-steady burning was not achieved during the droplet lifetime, as shown by the time-dependent burning rate and flame standoff ratios, which increased with time.
4. For hexanol concentrations above 10%, a soot shell was not visible. The soot shell standoff ratio increases with time and is always on the fuel-rich side of the flame.

Acknowledgments

The authors are pleased to acknowledge the support provided by NASA grant NAG 3-1791 (Dr. Merril King, Program Director, and Dr. Daniel Dietrich, Project Monitor). The authors would also like to acknowledge the advice and assistance of Prof. Francis Mcleod, helpful conversations with Professor Benjamin Shaw of the University of California (Davis), and Dr. Dietrich for providing the silica fibers.

REFERENCES

1. Okajima, S., and Kumagai, S., *Proc. Combust. Inst.* 15:401–407 (1975).
2. Avedisian, C. T., Yang, J. C., and Wang, C. H., *Proc. R. Soc. London A* 420:183–200 (1988).
3. Hara, H., and Kumagai, S., *Proc. Combust. Inst.* 25:423–430 (1994).
4. Choi, M. Y., Dryer, F. L., and Haggard, J. B., *Proc. Combust. Inst.* 23:1597–1604 (1990).
5. Nayagam, V., Haggard, J. B., Colantonio, R. O., Marchese, A. J., Dryer, F. L., Zhang, B. L., and Williams, F. A., *AIAA J.* 36:1369–1378 (1998).
6. Jackson, G. S., and Avedisian, C. T., *Proc. R. Soc. London A* 446:257–278 (1994).
7. Mikami, M., Niwa, M., Kato, H., Sato, J., and Kono, M., *Proc. Combust. Inst.* 27:439–446 (1998).
8. Chauveau, C., Chesneau, X., and Gokalp, I., *Adv. Space Res.* 16(7):157–160 (1995).
9. Marchese, A. J., Dryer, F. L., and Colantonio, R. O., *Proc. Combust. Inst.* 27:2627–2634 (1998).
10. Aharon, I., and Shaw, B. D., *Combust. Flame* 113:507–518 (1998).
11. Yang, J. C., Jackson, G. S., and Avedisian, C. T., *Proc. Combust. Inst.* 23:1619–1625 (1990).
12. Jackson, G. S., Avedisian, C. T., and Yang, J. C., *Proc. R. Soc. London A* 435:359–68 (1991).
13. Jackson, G. S., and Avedisian, C. T., *Int. J. Heat Mass Transfer* 41(16):2503–2515 (1998).
14. Aharon, I., and Shaw, B. D., *Microgravity Sci. Technol.* 10(2):75–85 (1997).
15. Okai, K., Tsue, M., Kono, M., Mikami, M., Sato, J., Dietrich, D. L., and Williams, F. A., *Proc. Combust. Inst.* 27:2651–2657 (1998).
16. Dietrich, D. L., Haggard Jr., J. B., Dryer, F. L., Nayagam, V., Shaw, B. D., and Williams, F. A., *Proc. Combust. Inst.* 26:1201–1207 (1996).
17. Tsue, M., Segawa, D., Kadota, T., and Yamasaki, H., *Proc. Combust. Inst.* 26:1251–1258 (1996).
18. Avedisian, C. T., *Combustion Science and Technology Book Series, Vol. 4,* Gordon and Breach Publishers, 1997, pp. 135–150.
19. Shaw, D. G. (ed.), *Solubility Data Series Hydrocarbons with Water and Seawater, Vol. 15.* Pergamon Press, Oxford, UK, 1984, pp. 263–290.
20. Shaw, D. G. (ed.), *Solubility Data Series Hydrocar-*

bons with Water and Seawater, Vol. 38, Pergamon Press, Oxford, UK, 1989, pp. 225–234.
21. Lide, D. R., *Basic Laboratory and Industrial Chemicals,* CRC Press, Ann Arbor, MI, p. 160, p. 229.
22. Cho, Y. S., Choi, M. Y., and Dryer, F. L., *Proc. Combust. Inst.* 23:1611–1617 (1990).
23. Marchese, A. J., and Dryer, F. L., *Combust. Sci. Technol.* 124:371–402 (1997).
24. Reid, R. C., Prausnitz, J. M., and Poling, B. E., *The Properties of Gases and Liquids, 4th ed.,* McGraw-Hill, New York, 1987.
25. Chao, B., Law, C. K., and T'ien, J. S., *Proc. Combust. Inst.* 23:523–531 (1990).
26. Mills, K., and Matalon, M., *Proc. Combust. Inst.* 27:2535–2541 (1998).
27. Struk, P. M., Dietrich, D. L., and T'ien, J. S., *Microgravity Sci. Technol.* 9(2):106–116 (1996).
28. Lee, K. O., Manzello, S. L., and Choi, M. Y., *Combust. Sci. Technol.* 132:139–156 (1998).
29. Choi, M. Y., and Lee, K. O., *Proc. Combust. Inst.* 26:1243–1249 (1996).
30. Jackson, G. S., Avedisian, C. T., and Yang, J. C., *Int. J. Heat Mass Transfer* 35:2017–2033 (1992).
31. Dietrich, D. L., and Haggard Jr., J. B., Second International Microgravity Combustion Workshop, NASA Conference Publication 10113, 317 (1992).
32. Lebedev, O. N., and Marchenko, V. N., *Heat Transfer Sov. Res.* 11:92–98 (1979).
33. Avedisian, C. T., and Jackson, G. S., *J. Prop. Power* 16 (in press).
34. Shaw, B. D., and Chen, A. G., *Microgravity Sci. Technol.* 10(3):136–143 (1997).
35. Callahan, B. J., and Avedisian, C. T., "Combustion of Nonane and Hexanol Droplets in Microgravity," Cornell Energy Report E-00-01.
36. Glassman, I., *Combustion,* Academic Press, San Diego, CA, 1987, pp. 274–275, 373–375.
37. Glassman, I., *Proc. Combust. Inst.* 27:1589–1596 (1998).
38. Sirignano, W. A., and Law, C. K., in *Advances in Chemistry Series 166* (J. T. Zung, ed.), 1978, pp. 3–26.
39. Struk, P. M., Dietrich, D. L., Sims, C., Picot, B., Kitano, K., Honma, S., Ikeda, K., and Ikegami, M., in *Proceedings of the First Joint Meeting of the U.S. Sections of the Combustion Institute,* Washington, DC, 1999, pp. 673–676.
40. Shaw, B. D., and Williams, F. A., *Int. J. Heat Mass. Transfer* 33:301–317 (1990).

COMMENTS

Cary Presser, NIST, USA. What would you expect the influence of other alcohol/nonane mixtures (such as with methanol in place of hexanol) to be on the point of initial soot suppression, as the alcohol content increases?

Author's Reply. We have not performed a systematic study of alcohol type on soot formation for spherical droplet flames. Methanol was the only other alcohol we examined in a previous study of methanol/toluene spherical droplet flames [1]. Our study kept the alcohol type fixed (hexanol) as well as the initial droplet diameter, and we varied the initial hexanol concentration in the droplet. As a result we can only speculate on what would happen if we changed the alcohol type in a systematic way for the spherically symmetric droplet burning process. Using arguments developed from laminar diffusion flames experiments [2], changing the alcohol type should change the gas-phase thermophysical properties (e.g., thermal diffusivity), as well as altering the chemical effect of the additive as it relates to forming soot precursor species. Alcohols lighter than hexanol, such as methanol, have a comparatively higher thermal diffusivity than hexanol and the droplet flame temperature should be lower; at the same time proportionally more oxygen is introduced into the gas phase. The result should be reduced soot compared to hexanol in nonane. Heavier alcohols should have thermal diffusivities lower than hexanol, and the chemical effect of the alcohol on suppressing soot formation should be diminished. As a result, the soot volume fraction should be higher relative to a hexanol/nonane droplet if other input parameters are the same. Complicating this speculation on the influence of alcohol type on soot suppression are other factors that could occur to varying degrees depending on the alcohol type but which were not observed for the hexanol/nonane combination such as microexplosions, extinction, absorption of water in the droplet, preferential vaporization, and two-stage burning.

REFERENCES

1. Jackson, G. S., Avedisian, C. T., and Yang, J. C., *Proc. R. Soc. Lond.* A435:359–368 (1991).
2. Glassman, I., *Proc. Combust. Inst.* 27:1589–1596 (1998).